International Journal of Mass Spectrometry 273 (2008) 58–68

Contents lists available at ScienceDirect

International Journal of Mass Spectrometry

journal homepage: www.elsevier.com/locate/ijms

Collision induced dissociation of deprotonated guanine: Fragmentation of pyrimidine ring and water adduct formation

Jassim Sultan*

Department of Chemistry, University of Guelph, Guelph, Ontario N1G 2W1, Canada

ARTICLE INFO

Article history:
Received 18 September 2007
Received in revised form 3 March 2008
Accepted 3 March 2008
Available online 13 March 2008

Keywords:
Guanine
Gas-phase reactions
Fragmentation pathways
Ketene
Fulvene

ABSTRACT

This investigation of collision induced dissociation of deprotonated guanine was conducted by using sequential ion trap tandem mass spectrometry and isotopically labelled guanine analogs to clarify the complex dissociation reactions of pyrimidine ring of deprotonated guanine. The fragmentation patterns confirmed that the gas-phase dissociation processes are initiated from the pyrimidine ring through charge site controlled reactions involving charge redistribution, proton transfer and nucleophilic attack to generate the three primary fragment products by the elimination of ammonia, cyanamide and isocyanic acid. Our findings shed light on the process of pyrimidine ring opening and closure prior to the decomposition of deprotonated guanine and therefore the identity of N1 and exocyclic N^2 is lost in deprotonated guanine as a result of scrambling. Intriguing association products of water addition to fragment ions have been structurally characterized to establish the role of ketene group in the selective gas-phase reaction of water addition and the formation of water adducts. The elimination of CO_2 from negatively charged water adducts provides evidence for the covalent attachment of water to the ketene moiety. The established mechanisms of the dissociation reactions of pyrimidine ring should provide a basis for the structural elucidation of guanine relevant species modified on its active sites. To lend support for our proposals, collision induced dissociation study of 8-phenyl-2′-deoxyguanosine adduct was performed.

1. Introduction

The fundamental importance of nucleobases and nucleosides has exceeded their primary role in cellular biology as the constituents of DNA and RNA. They are important cancer biomarkers [1,2] and their synthetic analogs are used as chemotherapeutic and antiviral agents [3,4]. Among all DNA bases, the guanine ring has the lowest oxidation potential [5] and thus is considered the primary target of many established carcinogens including alkylating and oxidizing agents [6], halogens [7] and phenoxyl and aromatic radicals [8]. In RNA, for example, there are more than 20 natural variants of guanine [9] which makes the structural differentiation between these compounds a challenging task.

The structural identification of guanine containing species by tandem mass spectrometry (MS) requires a fundamental understanding of the dissociation processes of guanine. Tandem MS and collision induced dissociation (CID) has been employed to study the dissociation reactions of positive ions of guanine [10–13]. In particular, complex gas-phase reactions of protonated guanine have been investigated by using ^{15}N and ^{18}O labelling [14], H/D exchange [15] and high performance mass spectrometry [16,17]. Negative ions of guanine have not received the attention given to positive ions as a result of the historical limitations of electrospray ionization (ESI) technique in the negative mode [15,18]. Tandem MS of deprotonated guanine had been reported [15,19] but the experimental approach based on a single stage mass analysis and H/D exchange did not provide sufficient information to elucidate the complex dissociation processes of deprotonated guanine.

This paper presents an in depth study of CID of deprotonated guanine using ESI ion trap tandem MS [20] and ^{15}N and ^{13}C isotopically labelled guanine analogs to elucidate the dissociation pathways, reaction mechanisms and structure of ions involved in the fragmentation of pyrimidine ring of deprotonated guanine. Gas-phase processes of negative ions are described in terms of charge site controlled reactions involving charge redistribution, proton transfer (PT) and nucleophilic attack. An understanding of the pyrimidine ring fragmentation of deprotonated guanine will facilitate the interpretation of the dissociation patterns of negative ions of guanine and modified guanine adducts and assist in the identification of many biological relevant molecules.

2. Experimental

2.1. Chemicals

Guanine was purchased from Aldrich Chemical Co. Inc. (Milwaukee, WI, USA). Dimethyl sulfoxide-d_6 (DMSO-d_6) and 8-^{13}C,

* Tel.: +1 519 824 4120x58110; fax: +1 519 766 1499.
E-mail address: jsultan@uoguelph.ca.

1387-3806/$ – see front matter © 2008 Elsevier B.V. All rights reserved.
doi:10.1016/j.ijms.2008.03.002

7,9-^{15}N guanine were purchased from Cambridge Isotope Laboratory Inc. (Andover, MA, USA). Guanosine amine-^{15}N was ordered from Icon Isotopes Inc. (Summit, NJ, USA). Hydrochloric acid was obtained from Sigma–Aldrich Canada Ltd. (Oakville, Ont., Canada). HPLC grade methanol, HPLC grade water, ammonium hydroxide and ammonium acetate were purchased from Fisher Scientific (Ottawa, Ont., Canada). Liquid nitrogen and helium were purchased from BOC Gases (Mississauga, Ont., Canada). 8-Phenyl-2′-deoxyguanosine adduct was provided by Dr. Richard A. Manderville.

2.2. Sample preparation

Guanosine amine-^{15}N (G15N2) and 8-phenyl-2′-deoxyguanosine (2DGPh) stock solutions at $\sim 10^{-3}$ M were prepared in water and 90:10 (v/v) methanol/water, respectively. The working solutions of G15N2 and 2DGPh at $\sim 10^{-5}$ M were prepared by diluting the stock solutions in 90:10 (v/v) methanol/water and adding 0.2% ammonium acetate (final concentration of ammonium acetate was ~0.5 mM). Guanine (G) and 8-^{13}C, 7,9-^{15}N guanine (G15N7,9) stock solutions at $\sim 10^{-3}$ M concentration were prepared in 0.15% HCl solution at a temperature of a water bath for 1 h. Working solutions of G and G15N7,9 at $\sim 10^{-5}$ M concentration were obtained by diluting the stock solutions in 90:10 (v/v) methanol/water and adding 1% NH_4OH solution to increase pH to ~8.

2.3. Mass spectrometry

Tandem MS experiments were performed on a Finnigan LCQ^{Deca} Ion Trap mass spectrometer. The sample solutions were continuously infused to the electrospray ionization (ESI) source by a syringe pump at a flow rate of 5 μL/min. The source was operated in the negative mode at −5.00 kV and the sample solutions were nebulized by using nitrogen as a sheath gas at a flow rate of 60 arbitrary unites (~0.9 L/min). The ions generated in ESI were transported into the ion optics region through the heated capillary at 200 °C. Ion optics parameters were optimized to provide the maximal ion transmission. All CID experiments were performed without automatic gain control (AGC) at an injection time of 15 ms with helium collision gas. The mass isolation window for all ions studied in tandem MS experiments was set at 1 *m*/*z*. Ion trap dissociation parameters; normalized collision energy (NCE), activation time (AT) and activation *q*, are provided in figure captions.

2.4. NMR spectroscopy

An NMR sample of G15N2 was prepared by dissolving 7.5 mg in 4 mL of DMSO-d_6. The 1D ^{1}H and 2D COSY and HSQC NMR experiments were carried out by using a Bruker Avance DPX-400 MHz spectrometer to verify the isotopic labelled site of G15N2 (spectra not shown).

3. Results and discussion

3.1. Deprotonated guanine ion generation [B–H]$^-$

Collision induced dissociation (CID) of guanine (G), 2-amino-^{15}N-guanosine (G15N2) and 8-^{13}C, 7,9-^{15}N guanine (G15N7,9) had been investigated by negative mode ESI ion trap tandem MS. The structure of G, G15N7,9 and G15N2 with atomic numbering are shown in Scheme 1A as 1, 2 and 3, respectively. CID spectra of the [B–H]$^-$ ions generated from G, G15N2 and G15N7,9 are shown in order in Fig. 1A–C. Deprotonated bases of G and G15N7,9 had been generated directly in the negative mode of the ESI by proton elimination at N9-H site from the neutral molecules. Guanine deprotonation mechanism had been established based on their gas-phase acidities [21,22], electrochemical measurements [23] and thermodynamic calculations [24,25]. Deprotonated nucleobase of G15N2 had been generated in the collision cell (MS^2) as a result of the elimination of the ribose moiety from deprotonated G15N2. Moreover, a characteristic mass shift of +1 Da was observed for [B–H]$^-$ of G15N2 which indicates the retention of the labelled nitrogen atom within the deprotonated base structure. Despite the differences in the formation mechanisms of [B–H]$^-$ from (G and G15N7,9) and G15N2, each process generates indistinguishable structure of [B–H]$^-$ with negative charge on N9 site [10,15], as illustrated in Scheme 1B.

3.2. Collision-induced dissociation of [B–H]$^-$

The dissociation of deprotonated guanine (*m*/*z* 150) proceeds through three previously established fragmentation pathways [15], as shown in Fig. 1A. Deammoniation (−17 Da, NH_3) is the major dissociation pathway to produce the product at *m*/*z* 133. The second dissociation pathway involves the elimination of cyanamide (−42 Da, H_2NCN) to generate the least abundant fragment at *m*/*z* 108. The last pathway is the expulsion of isocyanic acid (−43 Da, HNCO) to produce the product ion at *m*/*z* 107. In addition to these primary dissociation products, there were three intriguing fragment ions observed in the CID spectrum of [B–H]$^-$ at *m*/*z* 151, 126 and 82 which could not be generated directly from [B–H]$^-$ (*m*/*z* 150). Tandem MS experiments have shown that *m*/*z* 151 and 126 represent associated products of gas-phase water addition reaction to the precursor *m*/*z* 133 and 108 ions, respectively. The structural identification and the formation mechanisms of these ions will be discussed later.

The fragmentation products of *m*/*z* 153 ion of G15N7,9 are similar to those observed for the unlabelled G and a characteristic mass shift of +3 Da was observed for all ions detected, as shown in Fig. 1C. This concludes that all three isotopic atoms of the imidazole ring are retained within the structure of the fragment ions. Fig. 1B shows the CID spectrum of [B–H]$^-$ of G15N2 (*m*/*z* 151). The elimination of cyanamide shows the loss of the isotopically labeled nitrogen (−43 Da, $H_2NC^{15}N$) during the formation of *m*/*z* 108. Moreover, the elimination of the exogenic labeled nitrogen ($^{15}N^2$) as isocyanic acid (−44 Da, $H^{15}NCO$) had been established based on the formation of *m*/*z* 107. However, the deammoniation of G15N2 clearly shows two different dissociation pathways: the major dissociation pattern is associated with the generation of *m*/*z* 134 by the loss of the unlabelled ammonia (−17 Da, $^{14}NH_3$) and the second minor dissociation pattern produces *m*/*z* 133 by the elimination of the isotopically labeled ammonia (−18 Da, $^{15}NH_3$). The preferential loss of the unlabeled nitrogen at N1 site as $^{14}NH_3$ and the elimination of the isotopically labeled $^{15}N^2$ as isocyanic acid from G15N2 (Fig. 1B) concludes that the N1 and N^2 nitrogen atoms flip their positions and the order of these atoms is altered within the ionic structure of [B–H]$^-$ and thus this scrambling event is accountable for the two different dissociation pathways observed for the deammoniation of G15N2. Finally and similar to G and G15N7,9, three additional peaks had been detected at *m*/*z* 152, 126 and 82. The relative intensities of the CID products observed in Fig. 1 for G, G15N2 and G15N7,9 are summarized in Table 1.

The relative intensities of *m*/*z* 108 and 107 of G15N2 in Fig. 1B are altered compared to the corresponding peaks of G (Fig. 1A) and G15N7,9 (Fig. 1C) which thus suggests an overlap of more than one ion that shares the same nominal mass of *m*/*z* 108. Accordingly, the CID spectra of [B–H]$^-$ of G15N2 had been acquired at different NCE (0–30%) and were compared to those obtained for G, as shown in Fig. 2. CID of *m*/*z* 150 of G show that the generation of *m*/*z* 107 is initially observed at 20% NCE while the *m*/*z* 108 is detected later at

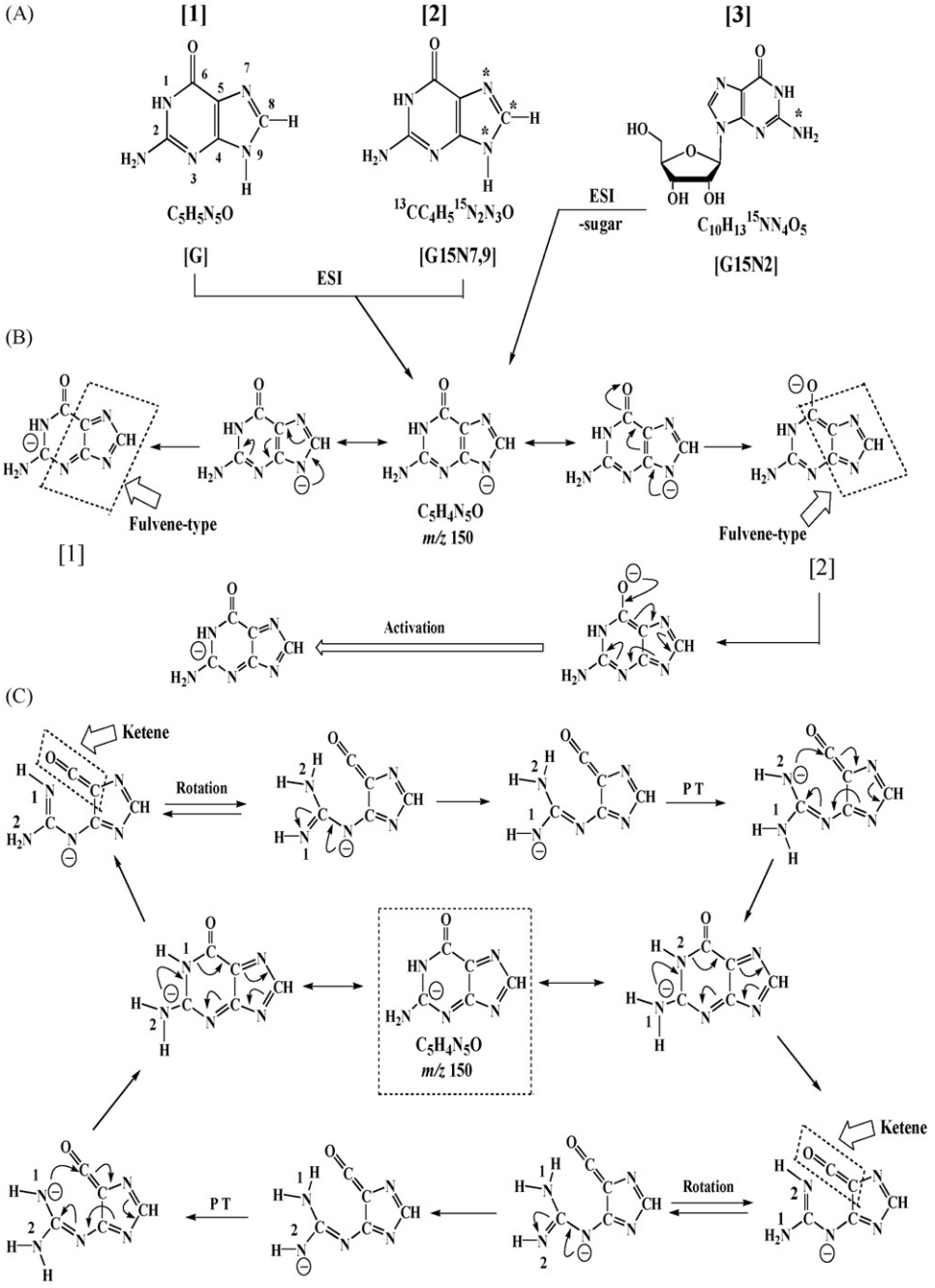

Scheme 1. (A) The structure of G, G15N7,9 and G15N2 with the atomic numbering. (B) A representation of charge redistribution during the activation of $[B–H]^-$ ion which creates fulvene-type moiety. (C) Proposed mechanism of pyrimidine ring opening and closing process which introduces the ketene moiety and causes the scrambling of N1 and N^2.

Table 1
The masses (*m*/*z*) with their relative intensities of the CID products observed for deprotonated guanine compounds

Compound	Loss		Ammonia (−17 Da)		Ammonia (−18 Da)				Cyanamide (−42 Da)		Cyanamide (−43 Da)				Isocyanic acid (−43 Da)		Isocyanic acid (−44 Da)	
	Parent	%	No label	%	Label	%	HP[a]	%	No label	%	Label	%	HP[b]	%	No label	%	Label	%
G	150	14.9	133	100.0	–		151	0.6	108	0.8	–		126	0.2	107	4.6	–	
G15N2	151	11.6	134	100.0	133[c]	3.5	152	0.6	–		108	0.8	126	0.2	108	3.8	107	1.4
G15N7,9	153	13.2	136	100.0	–		154	0.7	111	0.8	–		129	0.3	110	4.5	–	

[a] [b]Hydrated product ions of $[B–H–NH_3]^-$ and $[B–H–H_2NCN]^-$ fragments, respectively.
[c] The relative intensity of the hydrated product ion of *m*/*z* 133 fragment is negligible.

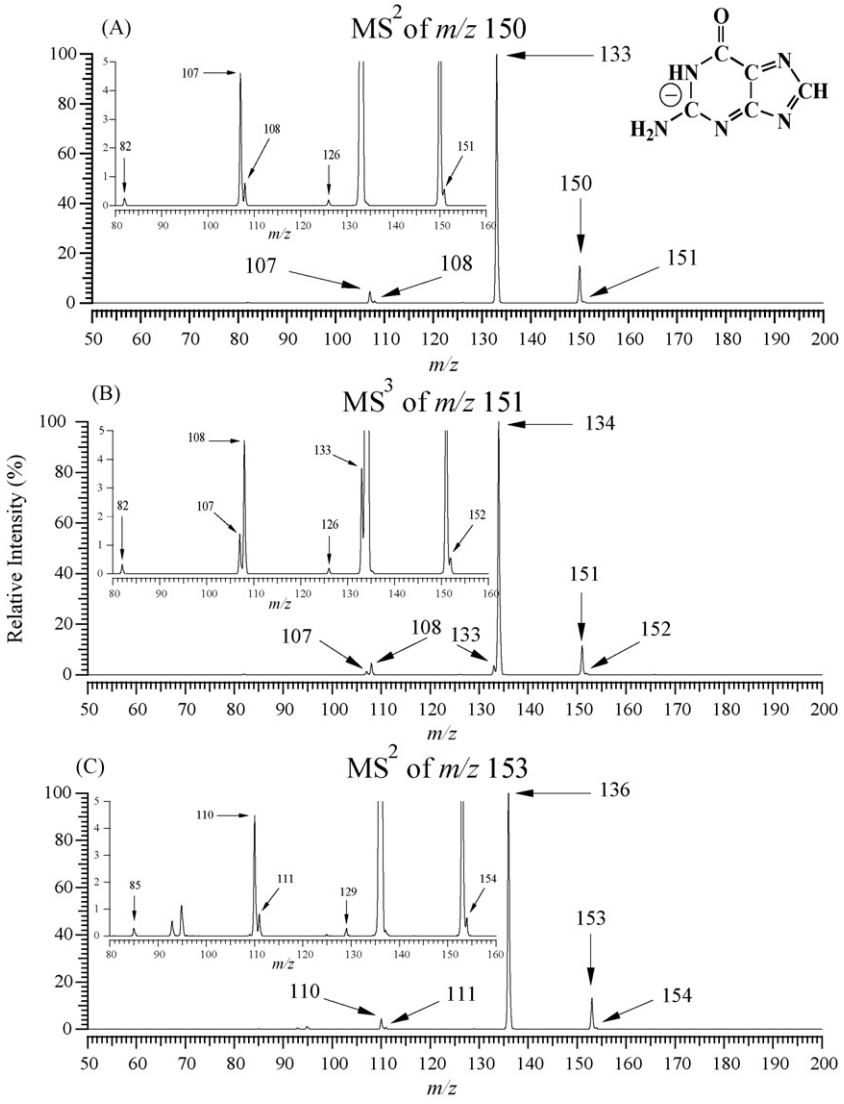

Fig. 1. Product ion spectra of deprotonated guanine standards acquired at 26% NCE, 30 ms AT and q value of 0.25. (A) m/z 150 of G. (B) m/z 151 of G15N2. (C) m/z 153 of G15N7,9.

higher NCE value of 25%, as illustrated in Fig. 2A. On the other hand, CID of m/z 151 of G15N2 in Fig. 2B show that m/z 107 and 108 were initially generated at 20% NCE and the peaks become more intense as the NCE is increased. Consequently, this comparison indicates that the m/z 108 peak presented in Fig. 1B at 26% NCE represents two different fragment products that are generated by the elimination of the unlabelled nitrogen at N1 as isocyanic acid (−43 Da, $H^{14}NCO$) and the loss of N1 and the isotopically labeled nitrogen ($^{15}N^{2}$) as cyanamide (−43 Da, $H_2NC^{15}N$).

The nominal mass overlap makes it difficult to precisely estimate the relative contribution of each fragment to the overall intensity of the diagnostic m/z 108 peak. This perplexity could be solved, to some extent, by using the crucial feature of m/z 108 (generated by the loss of cyanamide from G; Fig. 1A) which shows formation of m/z 126 as a result of gas-phase water addition. An examination of the relationship between the product ions at m/z 126 and 108 of G (Fig. 1A) shows that m/z 126 is detected at ∼25% of the intensity of m/z 108 (Table 1). The same relative intensity is expected to be between m/z 126 and 108 in G15N2 as m/z 108 generated from G and G15N2 are identical with no isotopic atom in their structure. Accordingly, the total relative intensity of m/z 108 generated by the loss of cyanamide from G15N2 in Fig. 1B is expected to be ∼0.8%. Consequently, the total contribution of the cyanamide dissociation pathway to the overall intensity of the diagnostic m/z 108 peak in the CID spectrum of G15N2 in Fig. 1B is ∼17%. This indicates that the unlabeled isocyanic acid expulsion pathway is the main source of m/z 108 of G15N2 in Fig. 1B. Furthermore, it shows that the elimination of the unlabeled isocyanic acid is more pronounced than the elimination of the isotopically labeled isocyanic acid which is similar to the pattern observed during the elimination of ammonia from G15N2 in Fig. 1B.

Dissociation reactions of $[B–H]^-$, similar to other charged bimolecular ions, are expected to be controlled by the location of the charge site [26,27]. Although the negative charge is initially accommodated on N9, the fragmentation patterns of $[B–H]^-$ confirmed that the dissociation processes are initiated from the pyrimidine ring which suggests the localization of the negative charge at that ring. The negative charge is expected to be delocalized to a certain degree throughout the conjugated double bonds of $[B–H]^-$ by resonance; however the charge distribution (or density) could be changed as a result of ion activation during the fragmentation processes. Two simplified representations of charge redistribution from N9 to the pyrimidine ring are proposed in Scheme 1B where the negative charge is expected to be localized

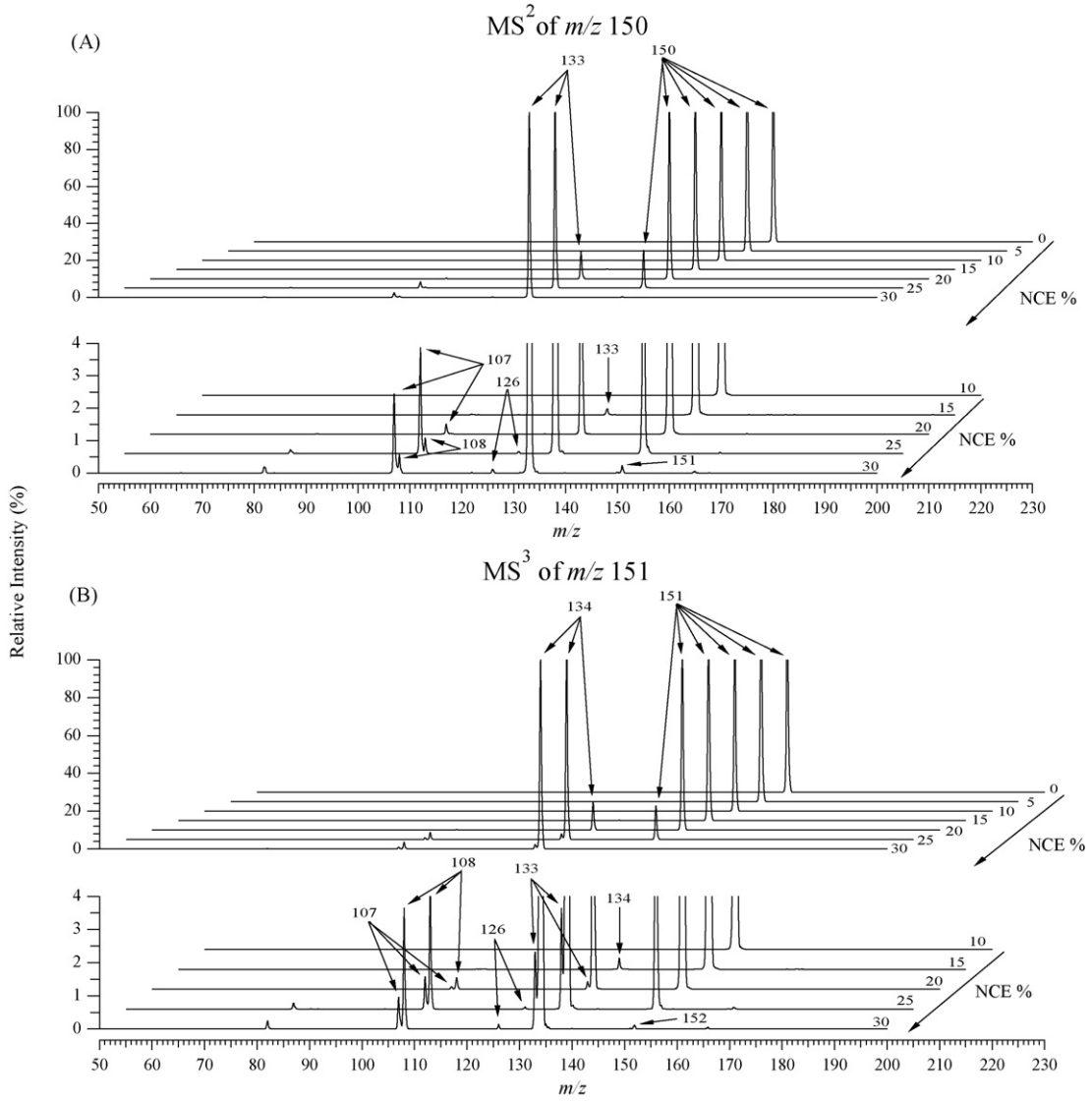

Fig. 2. CID energy profile spectra acquired at 30 ms AT and q value of 0.25 of (A) m/z 150 of G and (B) m/z 151 of G15N2.

on either oxygen or C2 of the pyrimidine ring. These activation processes create a *FULVENE*-type structure within the $[B–H]^-$ ion, meaning that the imidazole ring and N3 or C6 can be classified as a substituted fulvene ring and are presented in Scheme 1B as structure 1 and 2, respectively. Fulvene is usually described as a conjugated nonaromatic molecule [28,29] and the localization of its double bonds has been verified by spectroscopic studies [30,31]. Thus, applying the fulvene model on $[B–H]^-$ ion is expected to increase the charge density within the pyrimidine ring and suggests that the two fulvene-type rings may have a highly localized negative charge on oxygen and C2 as a result of the nonaromatic nature of the fulvene ring. Due to the higher electronegativity of oxygen, structure 2 is presumed to be the main abundant structure of $[B–H]^-$ in the collision cell.

The fragmentation patterns observed for $[B–H]^-$ ion in Fig. 1A suggest that the decomposition of the pyrimidine ring did not start from structure 2 (Scheme 1B), as this ionic structure fails to explain all the fragmentation products observed. For example, the elimination of isocyanic acid (HNCO) is difficult to envision from structure 2. However, the negative charge on oxygen in structure 2, during the activation of $[B–H]^-$, can be redistributed from oxygen throughout the entire imidazole ring to generate structure 1, as proposed in Scheme 1B. Therefore, it is assumed that the dissociation of pyrimidine ring occurs whenever the charge is accommodated on C2 of deprotonated guanine. The activation of $[B–H]^-$ is predicted to progressively increase the charge density on C2 until it reaches a point when opening of the pyrimidine ring occurs by breaking the amide N1/C6 bond and forming the open intermediate ionic structure of $[B–H]^-$ with localized negative charge on N3, as shown in Scheme 1C. Ring opening introduces a new reactive heterocumulene group into the ionic structure of $[B–H]^-$, namely *KETENE* ($R_1R_2C{=}C{=}O$). Ketene is defined as a neutral polarizable diatomic group with partial positive charge on carbonyl carbon, i.e. C6 of guanine, and it is very susceptible to nucleophilic attack [32]. Ring opening also allows free rotation of amino and imino groups along C2/N3 σ bond which changes the spatial orientation of each group with respect to C6 of the reactive ketene moiety. Redistribution of the negative charge from N3 to imine nitrogen N1, followed by a proton transfer from N^2 to N1 causes the reformation of the pyrimidine ring by nucleophilic attack of N^2 anion on C6 of ketene. The negative charge is expected to be accommodated on oxygen; however in activated $[B–H]^-$, the negative charge will redistribute itself again from oxygen to regenerate $[B–H]^-$ ion with localized negative charge on C2. This cycle of pyrimidine ring opening and closing is

expected to continue during the activation of $[B–H]^-$ ion until the collision energy is sufficient enough to decompose deprotonated guanine at the pyrimidine ring. The nitrogen scrambling observation (Fig. 1B) strongly suggest that pyrimidine ring opening and closure is a very fast electrocyclic process that proceed through the open intermediate structure by the cleavage of the amide C6/N1 σ bond, as proposed in Scheme 1C. The loss of 44 Da from *m*/*z* 151 ion of G15N2 in Fig. 1B is strong confirmation of pyrimidine ring closure after nitrogen scrambling.

Ring opening and closure indicates that deprotonated G ion exists in the collision cell as three structures. Two of them are closed structures that are distinguished by the reversed identity of N1 and N^2 as the exogenic amino group. The third structure is the intermediate ion with open pyrimidine ring. In the case of unlabelled G in Fig. 1A, the chemistry of N1 and N^2 are expected to be identical with respect to pyrimidine ring opening and closure and the identity of N1 and N^2 will be lost as a result of scrambling. Consequently, the dissociation processes of $[B–H]^-$ of unlabelled guanine proceed randomly from any of the two equivalent closed structures of deprotonated guanine.

Scheme 2A–C shows the proposed dissociation mechanisms of deprotonated G at *m*/*z* 150. The generation of the fragment ions at *m*/*z* 133 and 107 is initiated from the closed structure 1 with localized charge on C2. Repulsion between the negative charge localized on C2 and the electron lone pair of the exogenic nitrogen (N1 or N^2) atom increases the amino group basicity and leads to the loss of ammonia via four membered ring transition state and the formation of *m*/*z* 133 fragment ion with negative charge on C2, as proposed in Scheme 2A. The loss of isocyanic acid is initiated from structure 1 and proceeds through a concerted Retro Diels-Alder (RDA) mechanism with a six-membered cyclic transition state to generate the fragment ion at *m*/*z* 107 with localized negative charge on C2, as illustrated in Scheme 2B. However, the generation of the product ion at *m*/*z* 108 is expected to be initiated from the open intermediate of deprotonated G and is initiated by proton transfer from N1 (or N^2) to N3, followed by charge redistribution from N1 (or N^2) which leads to the loss of cyanamide and/or carbodiimide (HNCNH) and forming the *m*/*z* 108 ion with negative charge on N3, as proposed in Scheme 2C. The acidic properties of both amines and imines exhibit considerable variations [33] and thus both cyanamide and carbodiimide expulsion could be expected.

The preferential loss of $^{14}N1$ over $^{15}N^2$ observed in Fig. 1B of G15N2 as ammonia and isocyanic acid reflects the nitrogen isotopic effect on the dissociation of $[B–H]^-$. Isotopic substitution causes a variation in the dissociation reaction rate of the chemical bond that is formed or broken and is associated with kinetic isotopic effect (KIE) as a result of decreasing the vibrational frequency and zero-point energy of the chemical bond [34,35]. The vibrational frequency of the bond depends inversely on the reduced masses of the atoms that form the bond; therefore the bond with the heavier isotope will have a lower zero-point energy [35,36], which in turn increases the activation energy for the dissociation process that contains the heavier isotope [35,37]. Accordingly, the cleavage of the chemical bonds that contain the nitrogen isotope ($^{15}N^2$) is expected to require more energy than those having the nonisotopic atoms which consequently affects the formation rate of the dissociation products observed for $[B–H]^-$ of G15N2.

Although deammoniation and isocyanic acid expulsion pathways of G15N2 in Fig. 1B show preferential loss of the unlabelled $^{14}N1$, the elimination of $^{15}N^2$ was observed to vary with respect to the different fragmentation pathway. For example, the loss of ammonia shows that the fragment ion at *m*/*z* 133 is detected at ~3.5% of the intensity of *m*/*z* 134, while the loss of isocyanic acid shows that *m*/*z* 107 is detected at ~36% of *m*/*z* 108 (Table 1). The isotopic effect has a great outcome when the isotopic atom is involved in breaking (or forming) a bond due to primary isotopic effect [34,35] which is expected to be in both processes. However, the isotopic effect has been also linked to the structure and the type of chemical bond broken (or formed) [36] which could explain the variation observed between the two dissociation processes discussed above.

The elimination of isocyanic acid from G15N2 is envisioned to proceed through RDA mechanism from the closed pyrimidine ring. It is likely that the rate determining step during the elimination of

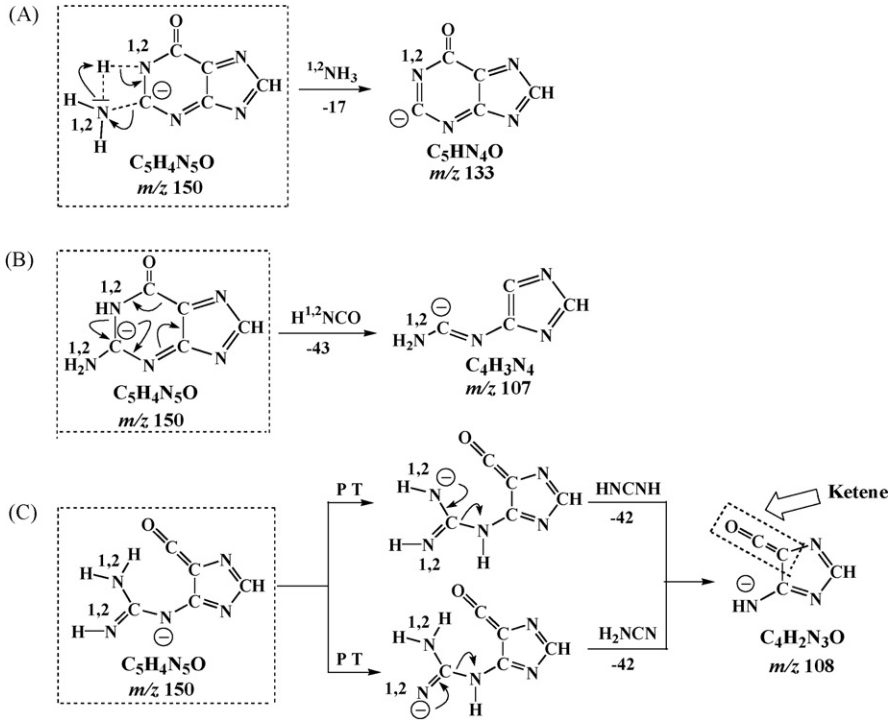

Scheme 2. Proposed dissociation patterns of deprotonated guanine.

isocyanic acid is breaking of the ^{14}N1/C2 or ^{15}N^2/C2 bond. The loss of isocyanic acid also involves bond breaking at C5/C6; however the effect of breaking this bond on both dissociation processes is identical and has no isotopic effect. Consequently, the preferential loss of the unlabeled isocyanic acid can be rationalized by the primary isotopic effect. The loss of ammonia involves the primary isotopic effect in the cleavage process of the exogenic ^{15}N^2/C2 and ^{14}N1/C2 bonds, however the isotopic effect is much more pronounced in this case. The huge difference in the preferential loss of the unlabelled ^{14}N1 as ammonia, compared to isocyanic acid, could be justified by the fact that the elimination process of ammonia is affected indirectly by the pyrimidine ring opening and closing process. This places the nitrogen isotope ^{15}N^2 inside the pyrimidine ring which consequently suggests that more energy must be supplied to break the ^{15}N^2/C6 bond to reopen the ring again and perform the reverse process (Scheme 1C). At the same level of energy, more of the nitrogen isotope ^{15}N^2 is expected to replace ^{14}N1 position inside the ring as a result of the isotopic effect. This is presumed to continue until the collision energy overcomes the activation energy required to break ^{15}N^2/C6 bond and reform the original structure of [B–H]$^-$. The activation energy differences shift the equilibrium towards formation of [B–H]$^-$ with the nitrogen isotope ^{15}N^2 inside the ring and ^{14}N1 outside the ring. The CID energy profile spectra presented in Fig. 2B show that the fragmentation of *m*/*z* 151 of G15N2 to generate *m*/*z* 134 fragment ion by the loss of unlabelled ammonia is initially detected at 15% NCE which is parallel to the NCE required for the deammoniation of unlabelled G observed in Fig. 2A. However, the loss of isotopically labeled ammonia from the original structure of G15N2 to produce *m*/*z* 133 product ion requires ~33% more energy and is observed later at 20% NCE. Furthermore, the elimination of labeled and unlabelled isocyanic acid from *m*/*z* 151 of G15N2 in Fig. 2B to produce in order *m*/*z* 107 and 108 fragment ions are initially detected at 20% NCE which is similar to the isocyanic acid dissociation pattern observed for G in Fig. 2A. These observations provide further evidence that the N1 and N^2 scrambling process occurs before the fragmentation of [B–H]$^-$ and demonstrates the equilibrium shift towards the formation of G15N2 with the ^{15}N^2 inside the pyrimidine ring as a result of the isotopic effect.

The heavier isotope also favors the chemical species where it is more strongly bonded [36] and thus the dissociation pattern of both the original and the reversed structure of [B–H]$^-$ of G15N2 are expected to vary as a result of the preferential retention of nitrogen isotope. Let us consider the two structures of [B–H]$^-$ of G15N2 as two different compounds and compare their dissociation patterns to those observed for [B–H]$^-$ of the unlabelled G in Fig. 1A where the intensity of *m*/*z* 107 ion relative to *m*/*z* 133 fragment was ~4.6% (Table 1). The fragmentation of the reversed structure of [B–H]$^-$ of G15N2 in Fig. 1B shows that *m*/*z* 107 fragment is detected at ~1.4% of *m*/*z* 134 ion (Table 1) which is consistent with the preferential cleavage of the exocyclic bond observed in Fig. 1A for the unlabelled G; moreover the isotopically labeled isocyanic acid dissociation pattern has been decreased as a result of the preferential retention of the nitrogen isotope. However, the decomposition of the original structure of [B–H]$^-$ of G15N2 observed in Fig. 1B shows two competitive dissociation pathways which initially occurs at the same NCE value of 20% (Fig. 2B) and generate the product ions at *m*/*z* 133 and 108 by the loss of the isotopically labelled ammonia and the unlabeled isocyanic acid, respectively. Consequently, the isotopically labeled deammoniation pattern has been decreased which strongly demonstrates the retention of the nitrogen isotope even though ^{15}N^2 is exocyclic to the pyrimidine ring. In summary, the favored elimination of the unlabelled ammonia is influenced by the primary isotopic effect on the exogenic bond; the favored retention of the nitrogen isotope and the secondary isotopic effect that arises from the indirect effect of the pyrimidine ring opening and closing.

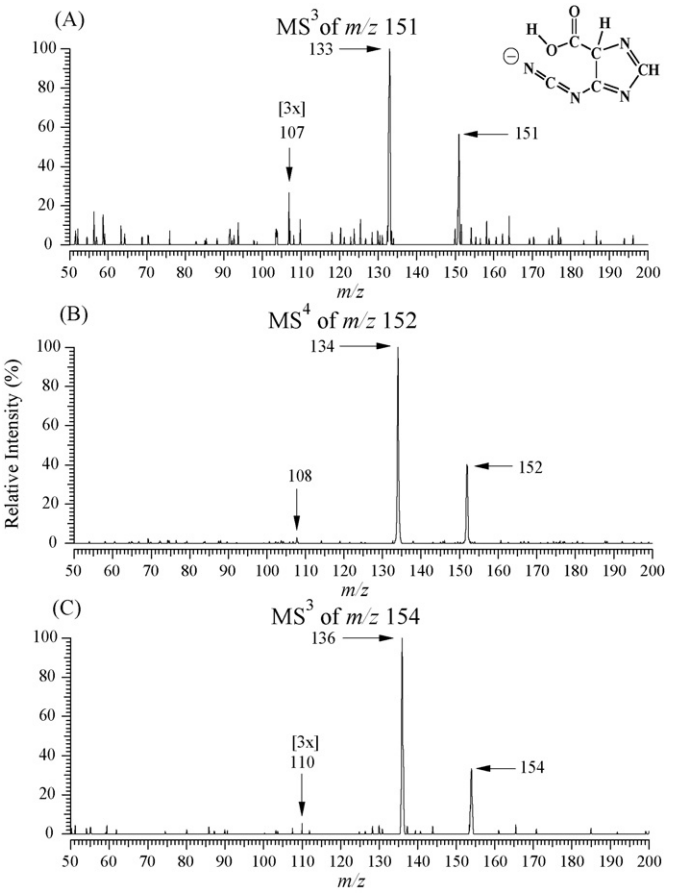

Fig. 3. Product ion spectra of water adduct of deaminated guanine acquired at 22% NCE, 20 ms AT, and *q* value of 0.30. (A) *m*/*z* 151 of G, (B) *m*/*z* 152 of G15N2 and (C) *m*/*z* 154 of G15N7,9.

Understanding the fragmentation mechanisms of pyrimidine ring clarified the dissociation pathways observed for guanine and shed light on the important process of pyrimidine ring opening and closure. Although this process produces identical structures in deprotonated guanine, pyrimidine ring opening and closure can potentially play an important role in the MS/MS identification of guanine and guanosine adducts modified at the pyrimidine ring.

In addition to formation of the primary dissociation products of G, CID spectra in Fig. 1 have shown fragment ions that could not be generated directly from [B–H]$^-$. The characterization of these intriguing ions has been accomplished based on their CID reactions where all ions exhibit characteristic losses of 18 and 44 Da which therefore excludes the involvement of all the isotopically labeled atoms in the neutral losses. The CID spectra of *m*/*z* 151 of G, *m*/*z* 152 of G15N2 and *m*/*z* 154 of G15N7,9 are shown in order in Fig. 3A–C. The dissociation of these ions shows a loss of 18 Da to generate *m*/*z* 133, 134 and 136 product ions, respectively, while the loss of 44 Da was marginal and generates the fragment ions at *m*/*z* 107, 108 and 110. The CID spectra of *m*/*z* 126 of G, 126 of G15N2 and 129 of G15N7,9 are shown in order in Fig. 4A–C. The decomposition of these ions demonstrates a major elimination of 44 Da which produces *m*/*z* 82, 82 and 85 product ions, respectively. A significant loss of 18 Da was also observed to produce the fragment ions at *m*/*z* 108, 108 and 111. Due to the similarity in the dissociation patterns observed for the three compounds, the discussion is limited to the fragment ions generated from deprotonated G.

The decomposition of *m*/*z* 151 and 126 of G has generated *m*/*z* 133 and 108 fragment ions, respectively. These ions (*m*/*z* 133 and 108) were observed earlier in the dissociation of *m*/*z* 150 of G in

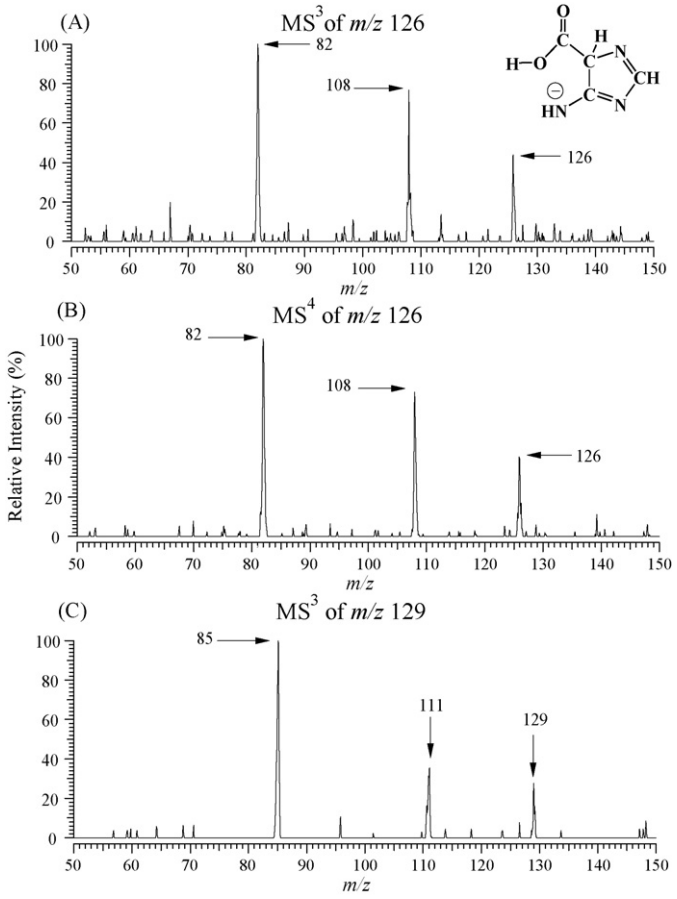

Fig. 4. Product ion spectra of water adduct of $[B–H–H_2NCN+H_2O]^-$ acquired at 27% NCE, 20 ms AT and q value of 0.35. (A) m/z 126 of G, (B) m/z 126 of G15N2 and (C) m/z 129 of G15N7,9.

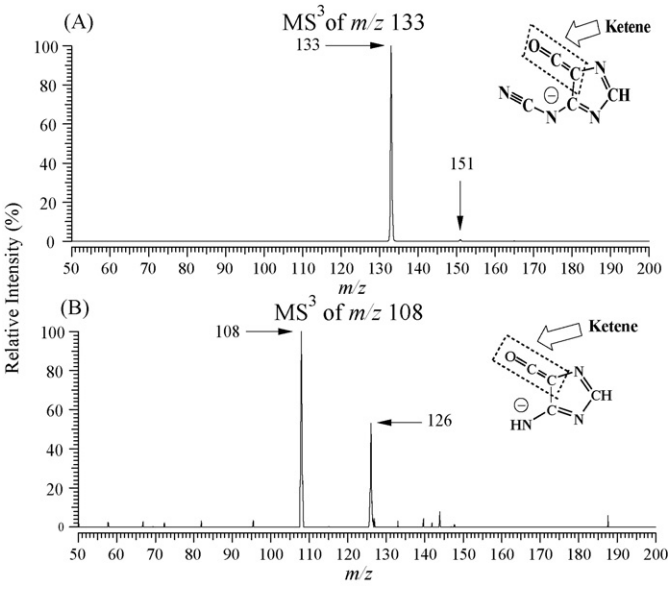

Fig. 5. Ion trap MS^3 spectra of (A) m/z 133 ion of G acquired at 0% NCE, 20 ms AT and q values of 0.30. (B) m/z 108 ion of G acquired at 0% NCE, 20 ms AT and q values of 0.35.

Fig. 1A which therefore suggests the involvement of m/z 133 and 108 fragments in the production of m/z 151 and 126 product ions, respectively. To investigate this effect, the CID spectra of m/z 133 and 108 ions have been acquired through the isolation of the precursor ions in the collision cell without applying any collision energy, i.e. 0% NCE. Interestingly, m/z 133 and 108 ions show the gain of 18 Da and generate m/z 151 and 126 product ions, as shown in Fig. 5A and B, respectively. The 18 Da gain/loss sequences suggest the addition of water to m/z 133 and 108 fragment ions. Water molecules accessible to adduct formation had been found to be delivered to the CID region by the collision gas and/or electrospray solvent [16,17].

3.3. Investigation of water gas-phase reaction

Observed selectivity of water attachment suggests a common structural feature shared by m/z 133 and 108 fragment ions that is susceptible to water addition and obviously is absent in m/z 107 fragment ion. The proposed structure of m/z 108 fragment ion in Scheme 2C contains a reactive ketene moiety which promptly reacts with water to form the hydrated product ion at m/z 126 as soon as m/z 108 fragment ion is generated at NCE value of 25%, as illustrated in Fig. 2A. However, the ketene moiety is absent in the proposed closed structure of m/z 133 in Scheme 2A which thus cannot participate in water attachment. Deaminated G (structure 2 of m/z 133 in Scheme 3A) has a similar structure as deprotonated G (Scheme 1C) with localized negative charge on C2 which suggests that activated m/z 133 ion could dissociate in a similar way as in deprotonated G. The pyrimidine ring opening in m/z 133 ion could proceed via reversed electrocyclic reaction, breaking N1(or N^2)/C6 bond and form the open structure 1, as shown in Scheme 3A. Another possible ring opening could proceed through RDA mechanism, breaking the C5/C6 bond and forms the open structure 3 (Scheme 3A). Structure 1 of m/z 133 contains the ketene moiety which can react with water to form m/z 151 product ion. Although pyrimidine ring opening of deprotonated G creates ketene moiety (Scheme 1C), water adduct had not been observed for $[B–H]^-$ (m/z 150) which reflects the fast nature of the ring opening and closure process.

Although both m/z 133 (structure 1 in Scheme 3A) and 108 fragment ions share the ketene group, the water addition reaction was observed to vary as shown in Fig. 5A and B. At 0% NCE, m/z 151 ion is detected at ~1% of the intensity of m/z 133 ion, while m/z 126 ion is detected at ~53% of m/z 108 ion. This large difference in water uptake gas-phase reaction concludes that m/z 133 ion mainly exists as a closed structure with no ketene character which lends support for the dissociation mechanisms and structural assignments proposed in Scheme 2A and C for m/z 133 and 108 fragment ions, respectively.

The proposed mechanisms of water addition reaction with m/z 133 and 108 fragment ions are shown in Scheme 3B and C, respectively. Nucleophilic attack of water on ketene's partially polarized C6 atom of m/z 133 and 108 leads, through a four membered ring transition state, to the formation of m/z 151 and 126 product ions. The proposed mechanisms involve transformation of ketene moiety into carboxylic acid group which implies a covalent nature of water attachment. It is important to note that the carboxylic acid group can change its spatial orientation with respect to N3 of m/z 108 and N1 (or N^2) of m/z 133 as a result of free rotation along C5/C6 σ bond. The 44 Da loss observed in Figs. 3 and 4, implies the elimination of CO_2 molecule from all water adducts containing the carboxylic acid group.

The elimination of water from m/z 151 is initiated by nucleophilic attack of N1 (or N^2) anion on the carboxyl carbon C6 which re-closes the pyrimidine ring and generates m/z 133 product ion with negative charge on C2, as shown in Scheme 4A. In a similar fashion, nucleophilic attack of N3 anion on the carboxyl carbon C6 expels water from m/z 126 ion and generates m/z 108 bicyclic product ion with negative charge accommodated on N9, as proposed in Scheme 4B. Although water elimination from m/z 151 and 126 ions is proposed to proceed through the same mechanism, the relative

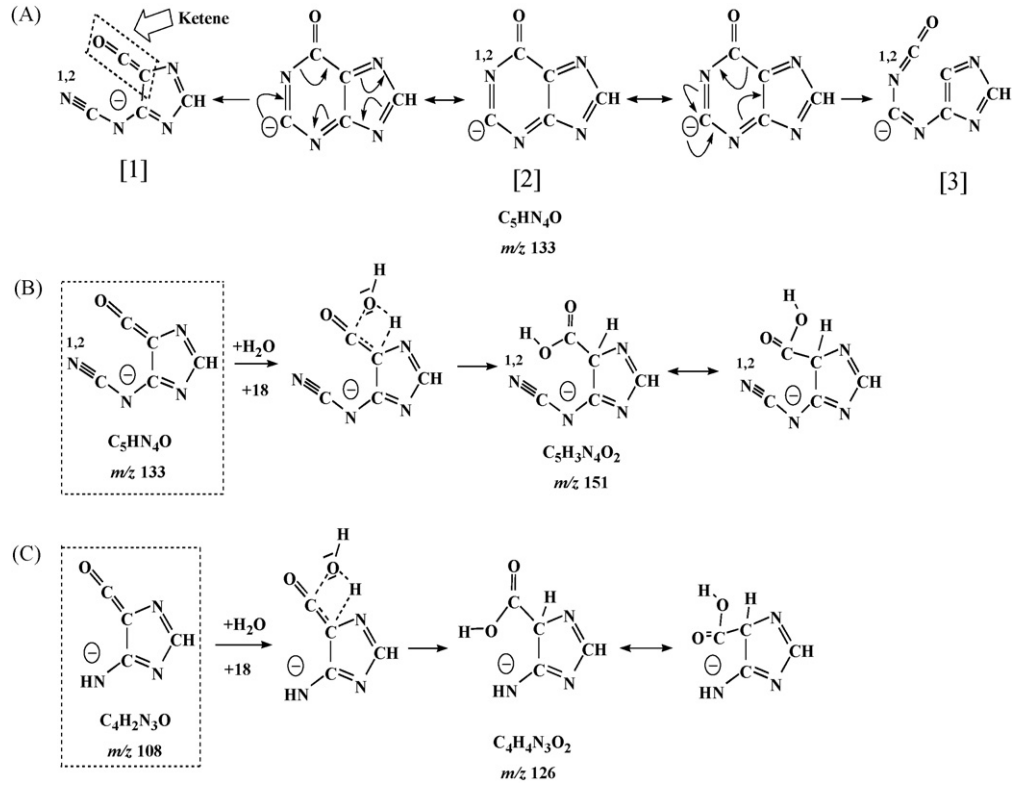

Scheme 3. (A) Proposed mechanism of pyrimidine ring opening of deaminated guanine ion. (B and C) Proposed mechanisms of gas-phase water addition reaction to *m*/*z* 133 and 108 fragment ions, respectively.

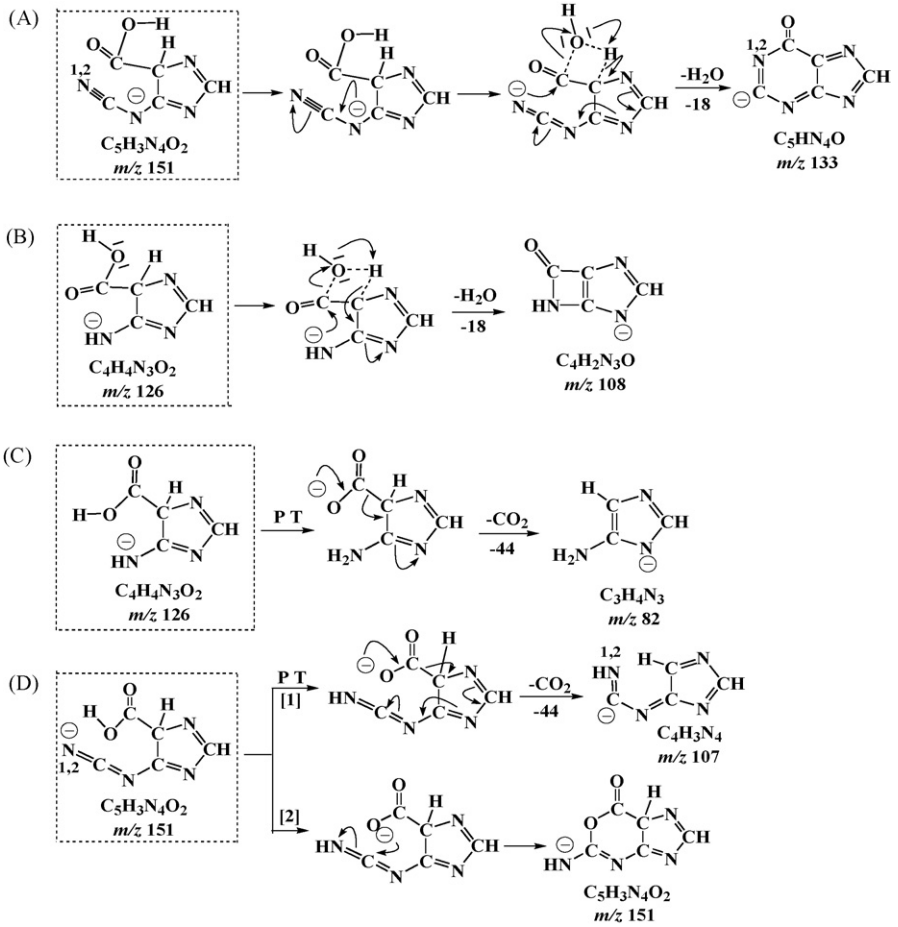

Scheme 4. Proposed dissociation patterns of *m*/*z* 151 and 126 water adducts of the respective *m*/*z* 133 and 108 fragment ions.

intensities of the fragmentation products were different. The variation observed is expected to be related to the intermediate structure in which water is eliminated. The elimination of water from *m*/*z* 126 ion, through a four member ring intermediate, is not as feasible as the elimination from *m*/*z* 151 ion which proceeds through a six member ring intermediate as a result of geometric (angel) strain associated with the formation of the four member ring.

The decarboxylation of *m*/*z* 126 ion is initiated by proton transfer from the carboxyl group to N3 and subsequent charge redistribution generates *m*/*z* 82 fragment ion with negative charge on N9, as illustrated in Scheme 4C. The CO_2 loss from *m*/*z* 151 is presumed to be initiated by proton transfer from the carboxyl group to N1 (or N^2) and subsequent charge redistribution which leads to the formation of *m*/*z* 107 fragment ion with negative charge accommodated on C2, as shown in Scheme 4D-1. The CO_2 loss from *m*/*z* 126 indicates that *m*/*z* 82 ion detected in Fig. 1A is generated directly from *m*/*z* 126 ion and not from *m*/*z* 150 ion. Moreover, the structure of *m*/*z* 107 generated from *m*/*z* 151 ion (Scheme 4D-1) is different from *m*/*z* 107 fragment ion generated from *m*/*z* 150 ion (Scheme 2B).

The elimination of CO_2 from *m*/*z* 151 was insignificant compared to the corresponding loss from *m*/*z* 126 which suggests that charge redistribution in carboxylate anion in *m*/*z* 151 ion may not be the predominant mechanism. This observation is consistent with the dissociation pattern obtained for several carboxylate anions originated from different hydroxycarboxylic acid compounds which show that the elimination of CO_2 is greatly influenced by the surrounding chemical (functional) species and surprisingly it may not detected at all [38]. In contrast to *m*/*z* 126 ion, the carboxylate anion

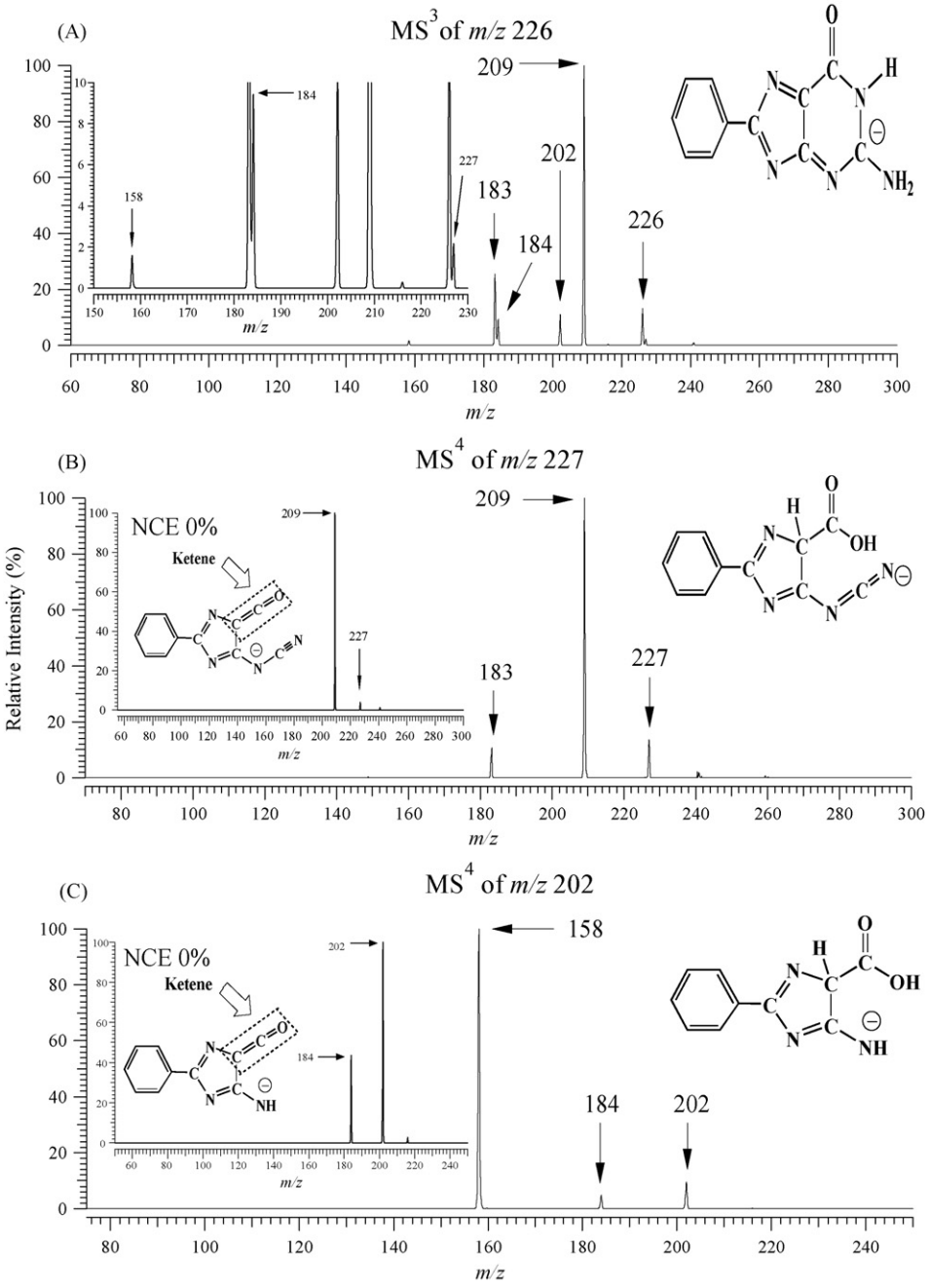

Fig. 6. Product ion spectra of 2DGPh of (A) *m*/*z* 226 ion acquired at 29% NCE, 30 ms AT and *q* value of 0.25. (B) *m*/*z* 227 acquired at 25% NCE, 20 ms AT and *q* value of 0.30. The inset shows the ion trap MS^4 spectra of *m*/*z* 209 at 0% NCE, 30 ms AT and *q* value of 0.25. (C) *m*/*z* 202 acquired at 29% NCE, 20 ms AT and *q* value of 0.35. The inset shows the ion trap MS^4 spectra of *m*/*z* 184 at 0% NCE, 30 ms AT and *q* value of 0.25.

in m/z 151 ion is in close proximity to carbodiimide moiety which could potentially initiate a nucleophilic attack on C2 of carbodiimide and form the lactone ring within the structure of m/z 151 ion and accommodate the negative charge on N1 (or N^2), as proposed in Scheme 4D-2. The new structure of m/z 151 ion is similar to deprotonated G and the elimination of CO_2 pathway could be compared to the isocyanic acid dissociation pathway which in turn suggests that the loss of CO_2 is expected to be small. Although CID experiments of m/z 107 ion (Fig. 3A) could not be performed due to its low abundance, the CO_2 loss from m/z 151 ion is believed to be preferentially initiated from the closed structure of m/z 151 intermediate as the nucleophilic addition reaction of carboxyl species on carbodiimide is relatively fast [39]. However, direct elimination of CO_2 by negative charge redistribution of the carboxylate anion (Scheme 2D-1), is still a possible dissociation pathway.

Understanding the gas-phase reactions of deprotonated G has clarified the dissociation pathways observed for several C8-2′-deoxyguanosine adducts studied in the context of our research. For example, as shown in Fig. 6A, the major dissociation pathways for the deprotonated base of 2DGPh (m/z 226) are similar to those observed for deprotonated G and proceed to produce the fragment products at m/z 209, 184 and 183 by the loss of ammonia, cyanamide and isocyanic acid, respectively. While the water uptake reactions of m/z 209 and 184 ions at 0% NCE generate in order the product ions at m/z 227 and 202, as shown in the inset of Fig. 6B and C. Furthermore, the dissociation of the hydrated product ions at m/z 227 and 202 exhibit characteristic losses of 18 and 44 Da to produce the fragment ions at (m/z 209 and 183) and (m/z 184 and 158), as shown in Fig. 6B and C. The characterization of these hydrated ions lends support to the role of ketene group in the selective gas-phase reaction of water addition and the dissociation reaction mechanisms proposed in Scheme 4.

Water adduct ions have been also observed in CID of protonated guanine [16,17]; however tandem MS of positively charged, hydrated fragment ions had only shown less informative elimination of water. The elimination of CO_2 and water from negatively charged hydrated ions were critical to establish the identity of the water adducts generated by the covalent attachment of water molecule to ketene group.

4. Conclusion

This investigation demonstrates the potential and selectivity of ion trap instrument for the collection of tandem MS data that clarified the complex fragmentation pathways of pyrimidine ring and elucidated the genealogical relationships for the CID products of deprotonated guanine. The key dissociation pathways, the reaction mechanisms and the structure of CID products have been also proposed. Gas-phase reactions of deprotonated guanine confirmed that the dissociation processes are initiated from the pyrimidine ring from localized negative charge site engaging the most labile activated ionic structure and proceed to generate the three primary fragment products by the elimination of ammonia, cyanamide and isocyanic acid. The dynamic process of pyrimidine ring opening and closure prior to the decomposition of deprotonated guanine has been confirmed by the investigation of the dissociation reactions of $^{15}N^2$ isotopically labelled G15N2 and therefore the identity of N1 and exocyclic N^2 is lost in guanine as a result of scrambling.

In addition to the major fragment ions, interesting products of water addition have been structurally characterized to establish the role of ketene group in the selective gas-phase reaction of water addition. The elimination of CO_2 from negatively charged water adducts provides evidence for the covalent attachment of water to the ketene moiety. Our findings provide new insights into the gas-phase chemistry of deprotonated guanine which can rationalize the fragmentation patterns observed and may provide a basis for the structural elucidation of guanine relevant species modified on its active sites.

Acknowledgements

This work was supported by the National Science and Research Council of Canada (NSERC) and Canada Foundation for Innovation (CFI). The author is very grateful to Dr. R.A. Manderville for providing 2DGPh.

References

[1] T.P. Waalkes, M.D. Abeloff, D.S. Ettinger, K.B. Woo, C.W. Gehrke, K.C. Kuo, E. Borek, Eur. J. Cancer Clin. Oncol. 18 (1982) 1267.
[2] E.P. Mitchell, L. Evans, P. Schultz, R. Madsen, J.W. Yarbro, C.W. Gehrke, K. Kuo, J. Chromatogr. 581 (1992) 31.
[3] C. Perigaud, G. Gosselin, J.L. Imbach, Bioorg. Med. Chem. Lett. 2 (1992) 677.
[4] C. Perigaud, G. Gosselin, J.L. Imbach, Nucleosides Nucleotides 11 (1992) 903.
[5] S. Bjelland, E. Seeberg, Mutat. Res. 531 (2003) 37.
[6] C.J. Burrows, J.G. Muller, Chem. Rev. 98 (1998) 1109.
[7] M. Masuda, T. Suzuki, M.D. Friesen, J.L. Ravanat, J. Cadet, B. Pignatelli, H. Nishino, H. Ohshima, J. Biol. Chem. 276 (2001) 40486.
[8] J.-A. Liu, C.J. Petzold, L.E. Ramirez-Arizmendi, J. Perez, H. Kenttamaa, J. Am. Chem. Soc. 127 (2005) 12758.
[9] P.A. Limbach, P.F. Crain, J.A. McCloskey, Nucleic Acids Res. 22 (1994) 2183.
[10] P.F. Crain, Mass Spectrom. Rev. 9 (1990) 505.
[11] J.M. Rice, G.O. Dudek, J. Am. Chem. Soc. 89 (1967) 2719.
[12] F.W. Crow, K.B. Tomer, M.L. Gross, J.A. McCloskey, D.E. Bergstrom, Anal. Biochem. 139 (1984) 243.
[13] M.G. Ikonomou, A. Naghipur, J.W. Lown, P. Kebarle, Biomed. Environ. Mass Spectrom. 19 (1990) 434.
[14] J.M. Gregson, J.A. McCloskey, Int. J. Mass Spectrom. Ion Processes 165 (1997) 475.
[15] A.M. Kamel, B. Munson, Eur. J. Mass Spectrom. 10 (2004) 239.
[16] R. Tuytten, F. Lemiere, W. Van Dongen, E.L. Esmans, E. Witters, W. Herrebout, B. Van Der Veken, E. Dudley, R.P. Newton, J. Am. Soc. Mass Spectrom. 16 (2005) 1291.
[17] R. Tuytten, F. Lemiere, E.L. Esmans, W.A. Herrebout, B.J. Van Der Veken, E. Dudley, R.P. Newton, E. Witters, J. Am. Soc. Mass Spectrom. 17 (2006) 1050.
[18] H. Hernandez, Rapid Commun. Mass Spectrom. 10 (1996) 1543.
[19] J.A. Hankin, R.C. Murphy, Anal. Biochem. 333 (2004) 156.
[20] R.E. March, J. Mass Spectrom. 32 (1997) 351.
[21] Y. Huang, H. Kenttamaa, J. Phys. Chem. A 108 (2004) 4485.
[22] E.C.M. Chen, C. Herder, E.S. Chen, J. Mol. Struct. 798 (2006) 126.
[23] S. Steenken, S.V. Jovanovic, J. Am. Chem. Soc. 119 (1997) 617.
[24] J.J. Christensen, J.H. Rytting, R.M. Izatt, Biochemistry 9 (1970) 4907.
[25] R.M. Izatt, J.J. Christensen, J.H. Rytting, Chem. Rev. 71 (1971) 439.
[26] M.T. Rodgers, S. Campbell, E.M. Marzluff, J.L. Beauchamp, Int. J. Mass Spectrom. Ion Processes 137 (1994) 121.
[27] S. Dua, J.H. Bowie, B.A. Cerda, C. Wesdemiotis, M.J. Raftery, J.F. Kelly, M.S. Taylor, S.J. Blanksby, M.A. Buntine, J. Chem. Soc., Perkin Trans. 2 (1997) 695.
[28] B.A. Hess, L.J. Schaad, J. Am. Chem. Soc. 93 (1971) 305.
[29] B.A. Hess, L.J. Schaad, J. Org. Chem. 36 (1971) 3418.
[30] J.F. Chiang, S.H. Bauer, J. Am. Chem. Soc. 92 (1970) 261.
[31] P.J. Domaille, J.E. Kent, M.F. O'Dwyer, Aust. J. Chem. 27 (1974) 2463.
[32] P. Sanchez-Andrada, I. Alkorta, J.A. Elguero, J. Mol. Struct. (Theochem) 544 (2001) 5.
[33] S. Hammerum, T.I. Solling, J. Am. Chem. Soc. 121 (1999) 6002.
[34] N.J. Turro, B. Kraeutler, in: E. Buncel, C.C. Lee (Eds.), Isotopes in Organic Chemistry, Elsevier, Amsterdam, 1984, p. 107.
[35] E.V. Anslyn, D.A. Dougherty, Modern Physical Organic Chemistry, University Science Books, California, 2006.
[36] J. Bigeleisen, Science 147 (1965) 4763.
[37] R.P. Bell, Chem. Soc. Rev. 4 (1974) 513.
[38] J. Sultan, W. Gabryelski, Anal. Chem. 78 (2006) 2905.
[39] T.L. Ibrahim, A. Williams, J. Chem. Soc., Perkin Trans. 2 (1982) 1459.